Optimal Eulerian model for the simulation of dynamics and coalescence of alumina particles in solid propellant combustion

François Doisneau, Frédérique Laurent, Angelo Murrone, Joel Dupays, Marc Massot

7th International Conference on Multiphase Flow,
ICMF 2010, Tampa, FL, May 30 – June 4, 2010

Optimal Eulerian model for the simulation of dynamics and coalescence of alumina particles in solid propellant combustion

François Doisneau*†, Frédérique Laurent-Nègre†, Angelo Murrone*,

Joël Dupays* and Marc Massot†

* Department of Fundamental and Applied Energetics, ONERA, 91120 Palaiseau, FRANCE

† Laboratoire EM2C, Ecole Centrale Paris and CNRS, 92295 Chatenay-Malabry, FRANCE

francois.doisneau@onera.fr, frederique.laurent@em2c.ecp.fr, angelo.murrone@onera.fr,

joel.dupays@onera.fr and marc.massot@em2c.ecp.fr

Keywords: Dilute Polydisperse Spray; Coalescence; Solid Propulsion; Alumina; Eulerian Multi-Fluid Model

Abstract

The accurate simulation of polydisperse sprays encountering coalescence in unsteady gaseous flows is a crucial issue for solid rocket booster optimization. Indeed, the internal flow of the engine depends strongly on the alumina droplet size distribution, which spreads up with coalescence. Yet solving for unsteady two-phase flows with a high dimensional phase space is a challenge for both modelling and scientific computing. The usual Lagrangian approaches lead to a very high computational cost or to a low resolution level and they induce coupling difficulties to the Eulerian gaseous phase description. A wide range of Eulerian models have been recently developed to describe the disperse liquid phase at a lower cost and with an easier coupling to the carrier gaseous phase. Among these models, the Multi-Fluid model allows the detailed description of polydispersity and size/velocity correlations by separately solving fluids of size-sorted droplets, the so-called sections. On the one hand, the existing first order description of the size distribution in each section provides simple and fast resolution for coalescence. On the other hand, a second order method allows to reduce the number of sections required to capture accurately coalescence and to use elaborate droplet collision modelling, yet at the cost of heavier computation algorithms. This paper seeks to conclude on computational time and precision of both methods in order to choose the most efficient configuration for multi-dimensional unsteady rocket chamber simulations. Its objective is threefold: first, to validate the second order method by comparing simulations to reference solutions and dedicated experimental measurements conducted at ONERA, second to study the efficiency and robustness of both methods on coalescing size-conditioned dynamics problems, third, to draw some firm conclusions about the necessity to use first order or second order methods in order to capture the physics of solid propulsion configurations.

Introduction

Two-phase flows constituted of a gaseous phase and a disperse condensed phase play a key role in many industrial and scientific applications : fuel atomization and evaporation by Diesel injectors; fluidized beds; gas bubbles in oil or boiling water pipeworks; dynamics of planet formation in solar nebulae; etc. In all these applications the disperse phase is composed of particles of various sizes that can eventually coalesce or aggregate, break-up, evaporate and have their own inertia and size-conditioned dynamics. So the importance of polydispersion is obvious for a full modelling of these phenomena.

In rocket boosters, aluminum powder is frequently used as solid propellant additive to increase specific impulse. Unlike the other ingredients, aluminum particles can burn in a significant portion of the chamber and produce a condensed liquid disperse phase of alumina. This disperse phase encounters drag forces, coalescence and heat exchanges (Dupays et al. 2000). In the nozzle, the droplets accelerate suddenly and cool down with the gas, becoming solid particles which break-up in such velocity gradients (Dukowicz 1980; O'Rourke 1981; Amsden et al. 1989). Thus, the disperse phase strongly interacts with the gaseous flow field during its way throughout the engine. It contributes to the booster performance loss, particularly via a decrease in nozzle efficiency; droplets are the source of slag material that

may remain in the engine during firing, causing insulation erosion in high concentration zones; some of the droplets, mainly the ones with high inertia which end up in the eventual aft-dome region around the submerged nozzle, induce sloshing motion of this molten liquid slag and can lead to control problems and possible vehicle instability. In such harsh conditions of pressure, temperature and velocity, solid propulsion experiments consume high technology materials and offer poor measurement output, especially on the disperse phase. The abundance of physical phenomena involved makes the models difficult to scale (Tòth 2008). Regarding the prohibitive cost of experiments, numerical simulation is the only available tool for optimizing rocket engines. Until now, complete 3D computations were achieved at the cost of drastic physics simplifications, allowing little self-reliance towards validation experiments. Yet time has come for comprehensive simulations, including advanced gas/droplet/structure coupled models, to give predictive answers.

Focusing on the dynamics of the alumina cloud in the combustion chamber is sufficient to evaluate specific impulse loss in the nozzle and slag material accumulation. Therefore the study takes place in the combustion chamber, where the principal physical processes that must be accounted for are : transport in real space, acceleration of droplets -due to drag conditioned by size- and coalescence, leading to polydispersity. These processes are remarkably sensitive to size distribution. We will therefore choose a model accurate as regards the size distribution and work with non-evaporating sprays throughout the paper, keeping in mind the broad application fields related to this study. By spray, we denote a disperse liquid phase constituted of droplets carried by a gaseous phase. We consider the specific case of dilute sprays i.e. where the liquid volume fraction is much smaller than one.

The retained approach called “mesoscopic” -or sometimes “kinetic” in reference to the kinetic theory of gases- describes the droplets as a cloud of point particles for which the exchanges of mass, momentum and heat are described using a statistical point of view, with eventual correlations : a finite set of global properties such as size of spherical droplets, velocity of the center of mass, temperature are modelled so that the total phase space is usually high-dimensional. More details about the droplets, such as angular momentum, can be predicted by increasing the size of the phase space : it is established that refined droplets models can be used as long as they do not include history terms. Williams (1958, 1985) proposed a transport equation based on kinetic theory that has proven to be useful for treating polydisperse, dilute and moderately dense liquid sprays. Such an equation describes the evolution of the number density function or NDF of the spray due to the drag force of the gaseous phase and the droplet-droplet interaction of coalescence (Kuentzmann 1973; Hylkema 1999; Laurent and Massot 2001; Laurent et al. 2004).

There are several strategies in order to solve the liquid phase and the major challenge in numerical simulations is to account for the strong coupling between all the involved processes. A first choice is to approximate the NDF by a sample of discrete numerical parcels of particles of various sizes through a Lagrangian-Monte-Carlo approach (Dukowicz 1980; O’Rourke 1981; Amsden et al. 1989; Hylkema 1999; Rüger et al. 2000). It is called Direct Simulation Monte-Carlo method (DSMC) by Bird (1994) and is generally considered to be the most accurate for solving Williams equation; it is specially suited for direct numerical simulations (DNS) since it does not introduce any numerical diffusion, the particle trajectories being exactly resolved. Its main drawback is the coupling of a Eulerian description for the gaseous phase to a Lagrangian description of the disperse phase, thus offering limited possibilities of vectorization/parallelization and implicitation. Besides, it brings another difficulty associated with the repartition of the mass, momentum and heat source terms at the droplet location onto the Eulerian grid for the gas description. Moreover for unsteady computations of polydisperse sprays, a large number of parcels in each cell of the computational domain is generally needed, thus yielding large memory requirement and CPU cost.

As an alternative, the Eulerian Multi-Fluid model, furthered by Laurent and Massot (2001); Laurent et al. (2004) from the ideas of Greenberg et al. (1993), relies on the derivation of a semi-kinetic modelling from the Williams equation using a moment method for velocity, but keeping the continuous size distribution function (Laurent and Massot 2001). This distribution function is then discretized using a "finite volume approach" in size phase space that yields conservation equations for mass, momentum (and eventually other properties such as number, energy) of droplets in fixed size intervals called sections, each of them constituting a different “fluid”. Please note that integrating on a continuous size variable in each section is a key aspect : while other Eulerian approaches often consider discrete droplet sizes gathered into “classes” which cannot account for the new droplet sizes created by coalescence (except scarce examples such as in Vasenin et al. (1995)), continuous size approaches such as the sectional method hereafter described are the only Eulerian methods handling coalescence naturally and rigorously. After integration on the sections, the resulting conservation equations are similar to those of the pressureless gas dynamics (Bouchut (1994); Zel′dovich (1970)) and lead to singu-

lar behaviors such as delta shocks and vacuum zones. Well-suited numerical methods are thus required, some specific schemes being presented in De Chaisemartin (2009). The model finally requires closure relations for the phenomena accounted for by the Williams equation. We refer to Abramzon and Sirignano (1989); Laurent and Massot (2001); Laurent et al. (2004) for detailed droplet models for which the Multi-Fluid model can be easily extended. These extensions do not have any impact on the conclusions of the present study.

The Eulerian Multi-Fluid model has proven its capability to simulate the size-conditioned dynamics of polydisperse sprays including coalescence with a first order resolution method of the size distribution in each section (Laurent and Massot 2001) even if the number of sections with the original method has to be large for accuracy purposes. In the context of evaporating sprays, several second order methods have been developed. A second order method using exponential size distributions in the sections is discussed in Laurent (2006). These two methods are in fact particular cases of a general method requiring n moments and introduced in Massot et al. (2010). The first order method can easily solve coalescence (Laurent et al. 2004) while the second order method has been extended to coalescence at the cost of some more elaborate algebra in Dufour (2005). It can yet easily include advanced models such as collision and coalescence efficiencies developed in Hylkema (1999); Hylkema and Villedieu (1998).

For the purpose of this paper, the first and second order methods have been implemented in a research code solving dilute sprays in a pseudo 2D nozzle with one-way coupling to the gaseous phase. The physical features have yet been simplified : the drag force is modelled by a Stokes law; the temperature, composition, density and viscosity of the gaseous phase are assumed to be constant and uniform; as a consequence unsteady heating of the droplets is negligible so that their temperature and density are also constant. This configuration is used to compare the two methods solving the dynamics and size evolution of a lognormal distributed spray. Moreover it fully validates the second order method by providing detailed comparisons to lagrangian and Multi-Fluid reference solutions. The research code also allows to simulate the complete dynamics of an experiment on coalescence (D'Herbigny and Villedieu 2001) which had been initially designed to validate collision efficiency models with an averaged analytical formula. This work is thus a continuation of the experiment exploitation and provides precious validation for such two-phase flow models, which too often lack experimental back up. Moreover this test case confirms the robustness of the method towards sharp or monodisperse distributions. These validations globally show the compliance of the second order Multi-Fluid method to the features required by rocket booster simulations i.e. accuracy on polydispersity and dynamics, advanced coalescence models, robustness and fast computation. In addition, the second order Multi-Fluid model had previously been featured in CEDRE, a multiphysics 3D industrial code developed at ONERA, the French aerospace lab. CEDRE provides fully coupled aero-thermochemical resolution for energetics problems. It includes advanced models and can therefore compute drag force, evaporation and coalescence terms depending on all the gas parameters. The paper thus presents rocket booster simulations performed with an optimized version of the second order Multi-Fluid to achieve the proof of the efficiency of such models in a complex physical background.

The paper is organized as follows. Section one is dedicated to the derivation of the Multi-Fluid method as a theoretical framework : the origin and assumptions of the corresponding coalescence models are detailed, as well as the resulting coalescence formulas for first and second order methods. In section two, we evaluate the accuracy/speed compromise provided by the two Multi-Fluid methods implemented in the research code on a simple pseudo-2D validation test case used in Laurent et al. (2004). In section three, we validate the second order Multi-Fluid method and its collision and coalescence efficiency models on a 1D coalescence efficiency experiment conducted at ONERA and detailed in D'Herbigny and Villedieu (2001). In section four, and to illustrate the ability of the second order model to simulate in a reasonable time a complete solid propulsion test case, we give some numerical results in a modelled chamber and nozzle using the CEDRE code before concluding the study.

1 Mesoscopic Eulerian spray modelling : two Multi-Fluid methods

In this section, we introduce the framework of our study : the kinetic description of the disperse phase and the derivation of two Eulerian resolution methods. The separation between the two methods appears when presuming the size distributions on the sections. The origin and assumptions of the corresponding coalescence models are widely detailed.

1.1 A kinetic description : the Williams equation

Number density function When focusing on polydispersity, the size parameter ϕ of droplets is of capital importance but its natural expression depends on the

phenomena : volume v is relevant towards conservation of matter, surface S towards evaporation and radius r towards impact factor for instance. Since we assume spherical droplets, equivalence relation $v = \frac{4}{3}\pi r^3 = \frac{1}{6\sqrt{\pi}} S^{\frac{3}{2}}$ allows the size to be expressed in this paper with the most comfortable notations.

Let us define the NDF function f^ϕ of the spray, where $f^\phi(t, \mathbf{x}, \mathbf{u}, \phi)\mathrm{d}\mathbf{x}\mathrm{d}\phi\mathrm{d}\mathbf{u}$ denotes the averaged number of droplets (in a statistical sense), at time t, in a volume of size $\mathrm{d}\mathbf{x}$ around a space location $\mathbf{x}$, with a velocity in a $\mathrm{d}\mathbf{u}$-neighborhood of $\mathbf{u}$ and with a size in a $\mathrm{d}\phi$-neighborhood of ϕ. As for the size parameter conversions, we shall keep in mind that $f^r(r)\mathrm{d}r = f^S(S)\mathrm{d}S = f^v(v)\mathrm{d}v$ and use the implicit notation f.

Williams equation The evolution of the spray is described by the Williams transport equation (Williams 1958). For a non evaporating case, it reads :

$$\partial_t f + \mathbf{u} \cdot \partial_{\mathbf{x}} f + \partial_{\mathbf{u}} \cdot (\mathbf{F}\, f) = \Gamma \tag{1}$$

where $\mathbf{F}$ is the drag force per unit mass and Γ is the coalescence source term.

As an illustration, the Stokes law models drag force $\mathbf{F}$ due to the velocity difference with the gaseous phase and reads :

$$\mathbf{F}(t, \mathbf{x}, \mathbf{u}, S) = \frac{\mathbf{U}(t, \mathbf{x}) - \mathbf{u}}{\tau_p(S)}, \quad \tau_p(S) = \frac{\rho_l S}{18\pi\mu_g}$$

where $\mathbf{U}$ is the gas velocity, μ_g represents its dynamic viscosity and ρ_l is the droplet (supposedly liquid) material density.

Coalescence operator The kinetic modelling for the collision operator leading to coalescence is taken from (Hylkema and Villedieu 1998). We then assume :

[C1] We only take into account binary collisions (small volume fraction of the liquid phase)

[C2] The mean collision time is very small compared to the intercollision time

[C3] During coalescence, mass and momentum are preserved.

Thus, $\Gamma = Q^+ - Q^-$ where Q^+ and Q^- respectively correspond to the quadratic integral operators associated with creation and destruction of droplets due to coalescence. These quadratic operators read (Hylkema and Villedieu 1998; Hylkema 1999):

$$\begin{aligned} Q^+ = & \frac{1}{2} \iint_{\mathbf{u}^\star, v^\star \in [0,v]} f(t, \mathbf{x}, \mathbf{u}^\diamond(v, v^\star, \mathbf{u}), v^\diamond(v, v^\star)) \times \\ & f(t, \mathbf{x}, \mathbf{u}^\star, v^\star) \mathfrak{B}(|\mathbf{u}^\diamond - \mathbf{u}^\star|, v^\diamond, v^\star) J \mathrm{d}v^\star \mathrm{d}\mathbf{u}^\star \\ Q^- = & \iint_{\mathbf{u}^\star, v^\star} f(t, \mathbf{x}, \mathbf{u}, v) f(t, \mathbf{x}, \mathbf{u}^\star, v^\star) \times \\ & \mathfrak{B}(|\mathbf{u} - \mathbf{u}^\star|, v, v^\star) \mathrm{d}v^\star \mathrm{d}\mathbf{u}^\star \end{aligned} \tag{2}$$

where $v^\diamond(v, v^\star) = v - v^\star$ and $\mathbf{u}^\diamond = \frac{v\mathbf{u} - v^\star \mathbf{u}^\star}{v - v^\star}$ are the pre-collisional parameters, J is the Jacobian of the transform $(v, \mathbf{u}) \to (v^\diamond, \mathbf{u}^\diamond) : J = (v/v^\diamond)^d$ with d the dimension of the velocity phase space and $B(|\mathbf{u} - \mathbf{u}^\star|, v, v^\star)$ is the collision/coalescence probability kernel which reads :

$$\mathfrak{B}(|\mathbf{u} - \mathbf{u}^\star|, v, v^\star) = \mathfrak{E}(|\mathbf{u} - \mathbf{u}^\star|, v, v^\star)\ |\mathbf{u} - \mathbf{u}^\star|\ \beta(v, v^\star)$$

In this kernel, $\beta(v, v^\star) = \pi\,(r + r^\star)^2$ is the impact parameter and $\mathfrak{E} = \mathfrak{E}_{\text{coll}}.\mathfrak{E}_{\text{coal}}$ accounts for the collision efficiency $\mathfrak{E}_{\text{coll}}$ and the coalescence efficiency $\mathfrak{E}_{\text{coal}}$. The modelling of these efficiencies is detailed in the following two paragraphs.

Collision efficiency Collision efficiency $\mathfrak{E}_{\text{coll}}$ is a probability factor modelling the correlation of droplet velocities immediately before a collision. It is equivalent to consider that droplets may dodge each other due to the gas flow surrounding them. Collision efficiency laws thus require knowledge of local gas parameters such as density ρ_g or viscosity μ_g.

In the case of unbalanced droplet sizes, D'Herbigny and Villedieu (2001) select two collision efficiency models : the Langmuir-Blodgett model, and the Beard-Grover model (Hylkema 1999; Achim 1999). These laws strongly depend on the bigger droplet Reynolds number and on a dimensionless number k which read, when taking r_1 the smaller radius and r_2 the bigger radius :

$$Re = \frac{2\rho_g r_2}{\mu_g}\ |\ \mathbf{U} - \mathbf{u}_2\ |\ , \qquad k = \frac{2\rho_l r_1^2 |\mathbf{u}_2 - \mathbf{u}_1|}{9\mu_g r_2}$$

The number k is the ratio of the smaller droplet relaxation time $\tau_r = \frac{2\rho_l r_1^2}{9\mu_g}$ to its residence time in the bigger droplet influence zone $\tau_h = \frac{r_2}{|\mathbf{u}_2 - \mathbf{u}_1|}$.

In the case of low Reynolds numbers, Langmuir and Blodgett (Langmuir 1948) numerically get the following expression :

$$\begin{cases} E_1(k) = 0 & \text{if } k \leq 1.214 \\ E_1(k) = \left(1 + \frac{3\ln(2k)}{2(k-1.214)}\right)^{-2} & \text{otherwise} \end{cases}$$

whereas for high Reynolds, they get :

$$\begin{cases} E_2(k) = 0 & \text{if } k \leq 0.0833 \\ E_2(k) = \frac{k^2}{(k+0.5)^2} & \text{otherwise} \end{cases}$$

For intermediate cases they assume the following interpolation :

$$\mathfrak{E}_{\text{coll}}^{\text{LB}}(k, Re) = \frac{E_1(k)}{1 + Re/60} + \frac{(Re/60)E_2(k)}{1 + Re/60} \quad (3)$$

Beard and Grover (1974) suggest to increase the accuracy of formula (3) which results from a simple interpolation between two limits. For this purpose, they use a numerical solution of the incompressible Navier-Stokes equations in order to determine the gaseous flow surrounding the bigger droplet depending on the Reynolds number. They can therefore evaluate precisely the forces on the smaller droplet and compute its trajectory. For $Re \in [0, 400]$ and $r_1 < r_2$, it yields:

$$\mathfrak{E}_{\text{coll}}^{\text{BG}}(k, Re) = \frac{4}{\pi^2}[\arctan(\max(H(k, Re), 0))]^2 \quad (4)$$

where

$$H = 0.1465 + 1.302Z - 0.607Z^2 + 0.293Z^3$$
$$Z = \ln(k/k_0)$$
$$k_0 = \exp(-0.1007 - 0.358\ln(Re) + 0.0261[\ln(Re)]^2)$$

Typical collision efficiency values with these two laws are in Fig. 1.

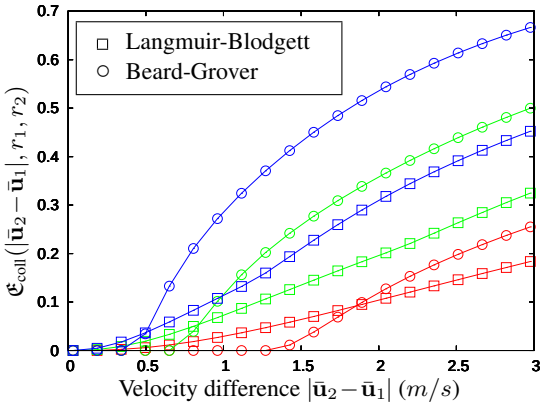

Figure 1: Two collision laws selected for booster applications with $r_2 = 150\mu m$ (red : $r_1 = 2\mu m$, green : $r_1 = 3\mu m$; blue : $r_1 = 4\mu m$)

Coalescence efficiency Coalescence efficiency $\mathfrak{E}_{\text{coal}}$ is the probability for two droplets to merge after a collision. Since the droplets can bounce on each other or separate by reflexion or stretching if the remaining kinetic energy of the new droplet is too high, coalescence efficiency depends *a priori* on the velocity parameters, the droplet material viscosity and surface tension, etc.

Most simple laws such as the Brazier-Smith model (Achim 1999; Brazier-Smith et al. 1972) are commonly used. Especially, the CEDRE code provides this model but it is not used in the following simulations. Therefore, the Brazier-Smith model is not detailed any further.

The formalism and the associated assumptions needed to derive the Eulerian Multi-Fluid models are introduced in Laurent and Massot (2001). We shall now recall the two main steps which are the semi-kinetic derivation and the sectional integration in order to precisely introduce the coalescence terms.

1.2 Semi-kinetic model

Velocity coherence assumption In a first step we reduce the size of the phase space, considering only the moments of order zero and one in the velocity variable at a given time, a given position and for a given droplet size : $n = \int f d\mathbf{u}$ and $\bar{\mathbf{u}} = \int \mathbf{u} f d\mathbf{u}/n$ which depends on $(t, \mathbf{x}, S)$. In order to close the system, the following assumptions are introduced :

[H1] For a given droplet size, at a given point $(t, \mathbf{x})$, there is only one characteristic averaged velocity $\bar{\mathbf{u}}(t, \mathbf{x}, S)$.

[H2] The dispersion around the averaged velocity $\bar{u}(t, \mathbf{x}, S)$ is zero in each direction, whatever the point $(t, \mathbf{x}, S)$.

It is equivalent to presume the following NDF :

$$f(t, \mathbf{x}, \mathbf{u}, S) = n(t, \mathbf{x}, S)\delta(\mathbf{u} - \bar{\mathbf{u}}(t, \mathbf{x}, S))$$

The monokinetic hypothesis [H1] is equivalent to reducing the velocity distribution support to a one dimensional submanifold parameterized by droplet size. It is fairly correct when the Stokes number is small enough for the droplets to follow the flow (Massot 2007). Yet it prevents droplet-crossing, which can occur in solid propulsion during ejection from fast vortices or high speed parietal injection.

The zero-dispersion hypothesis [H2] is justified when neither turbulence nor brownian phenomena interact with the disperse phase.

These hypotheses thus induce strong limitations for rocket booster simulation and will be discussed in the conclusion of this paper.

Equations This step leads to a system of conservation equations called the semi-kinetic model; it is a mono-kinetic model, saying that at a fixed position and time and for a fixed size, there is only one possible velocity. The semi-kinetic system reads :

$$\begin{aligned} \partial_t n + \partial_{\mathbf{x}} \cdot (n\bar{\mathbf{u}}) &= Q_n^+ - Q_n^- \\ \partial_t(n\bar{\mathbf{u}}) + \partial_{\mathbf{x}} \cdot (n\bar{\mathbf{u}} \otimes \bar{\mathbf{u}}) &= n\bar{\mathbf{F}} + Q_u^+ - Q_u^- \end{aligned} \quad (5)$$

Semi-kinetic coalescence operator In the semi-kinetic framework, the coalescence operator yields the evolution rate of the zeroth and first order moments of the velocity phase space. These two terms read, when omitting the $(t, \mathbf{x})$ dependency :

$$\begin{aligned} Q_n^+ &= \frac{1}{2}\int_{v^\star\in[0,v]} n(v^\diamond(v,v^\star))n(v^\star)\beta(v^\diamond,v^\star)I_n^+\mathrm{d}v^\star \\ Q_n^- &= -n(v)\int_{v^\star\in[0,+\infty[} n(v^\star)\beta(v,v^\star)I_n^-\mathrm{d}v^\star \\ Q_u^+ &= \frac{1}{2}\int_{v^\star\in[0,v]} n(v^\diamond(v,v^\star))n(v^\star)\beta(v^\diamond,v^\star)I_u^+\mathrm{d}v^\star \\ Q_u^- &= -n(v)\int_{v^\star\in[0,+\infty[} n(v^\star)\beta(v,v^\star)I_u^-\mathrm{d}v^\star \end{aligned} \tag{6}$$

where I_n^-, I_n^+, I_u^- and I_u^+ are the partial collisional integrals. To preserve the monokinetic and zero-dispersion assumptions, these integrals are computed with average velocities and therefore read :

$$\begin{aligned} I_n^+ =& |\bar{\mathbf{u}}(v^\star)-\bar{\mathbf{u}}(v^\diamond)|\ \mathfrak{E}(|\bar{\mathbf{u}}(v^\star)-\bar{\mathbf{u}}(v^\diamond)|,v,v^\star) \\ I_n^- =& |\bar{\mathbf{u}}(v)-\bar{\mathbf{u}}(v^\star)|\ \mathfrak{E}(|\bar{\mathbf{u}}(v)-\bar{\mathbf{u}}(v^\star)|,v,v^\star) \\ I_u^+ =& \frac{(v^\diamond\bar{\mathbf{u}}(v^\diamond)+v^\star\bar{\mathbf{u}}(v^\star))}{(v^\star+v^\diamond)}\times \\ & |\bar{\mathbf{u}}(v^\star)-\bar{\mathbf{u}}(v^\diamond)|\ \mathfrak{E}(|\bar{\mathbf{u}}(v^\star)-\bar{\mathbf{u}}(v^\diamond)|,v,v^\star) \\ I_u^- =& \bar{\mathbf{u}}(v)\ |\bar{\mathbf{u}}(v)-\bar{\mathbf{u}}(v^\star)|\ \mathfrak{E}(|\bar{\mathbf{u}}(v)-\bar{\mathbf{u}}(v^\star)|,v,v^\star) \end{aligned}$$

1.3 Multi-Fluid model

In a second step we choose a discretization $0 = S_0 < S_1 < \cdots < S_N$ for the droplet size phase space and we average the system of conservation laws over each fixed size interval $[S_{k-1}, S_k[$, called section. The set of droplets in one section can be seen as a "fluid" for which conservation equation are written, the sections exchanging mass and momentum. In order to close the system, the following assumptions are introduced :

[H3] In one section, the characteristic averaged velocity does not depend on the size of the droplets.

[H4] The form of n as a function of S is supposed to be independent of t and $\mathbf{x}$ in a given section, thus decoupling the evolution of the mass concentration of droplets in a section from the repartition in terms of sizes.

These assumptions are equivalent to presuming the NDF in velocity and size inside each section k :

$$\forall S\in[S_{k-1},S_k[\ \left\{\begin{array}{l}\bar{\mathbf{u}}(t,\mathbf{x},S)=\bar{\mathbf{u}}_k(t,\mathbf{x})\\ n(t,\mathbf{x},S)=\kappa_k(t,\mathbf{x},S)\end{array}\right.$$

Since we have chosen a constant value for the velocity distribution in each section, Multi-Fluid methods based on assumption [H3] feature a first order velocity convergence with the number of sections. It induces a convenient integration simplification but it can generate trajectory modes. For coarse size discretizations indeed, it assumes the same velocity for droplets of remarkably different sizes in a given section.

As for [H4], it allows to reduce the size distribution information of each section at $(t, \mathbf{x})$ to a set of moments of S, the number of which depends on the choice of the $(\kappa_k)_k$ set of functions. The difference between the two methods we are about to introduce is yet the choice of their form.

In the so-called first order method, a constant ${}^1\kappa_k$ function in each section yields a first order granulometry convergence with the number of sections. Whereas in the second order method, a two-coefficient ${}^2\kappa_k$ function yields a second order granulometry convergence. The choice of refining the size distribution description is of course related to the need of a fine resolution of polydispersity, as told in introduction.

1.4 First order method

First order size assumption The first order Multi-Fluid method assumes, instead of [H4], the following notation in each section k :

$$n(t,\mathbf{x},S) = m_k(t,\mathbf{x})\,{}^1\kappa_k(S)$$

where m_k is the mass concentration of droplets in the k^{th} section, in such a way that

$$\int_{S_{k-1}}^{S_k} {}^1\kappa_k(S)\frac{\rho_l}{6\sqrt{\pi}}S^{3/2}\mathrm{d}S = 1.$$

Such an approach only focuses on one moment of the distribution in the size variable : the moment in terms of mass is chosen because it is conserved by coalescence.

Please note that the distribution on the last section is a decreasing exponential with a fixed coefficient. This choice allows the final section to treat the bigger droplets but requires not to have a significant part of the mass. This is a major limitation compared to the second order method.

Equations The conservation equations for the k^{th} section result from the integration of the mass moment of the semi-kinetic system (5) in each section k and reads :

$$\begin{aligned} \partial_t m_k + \partial_{\mathbf{x}}\cdot(m_k\bar{\mathbf{u}}_k) &= {}^1\mathbf{C}_k^{m+} - {}^1\mathbf{C}_k^{m-} \\ \partial_t(m_k\bar{\mathbf{u}}_k) + \partial_{\mathbf{x}}\cdot(m_k\bar{\mathbf{u}}_k\otimes\bar{\mathbf{u}}_k) &= m_k\bar{\mathbf{F}}_k + {}^1\mathbf{C}_k^{mu+} - {}^1\mathbf{C}_k^{mu-} \end{aligned} \tag{7}$$

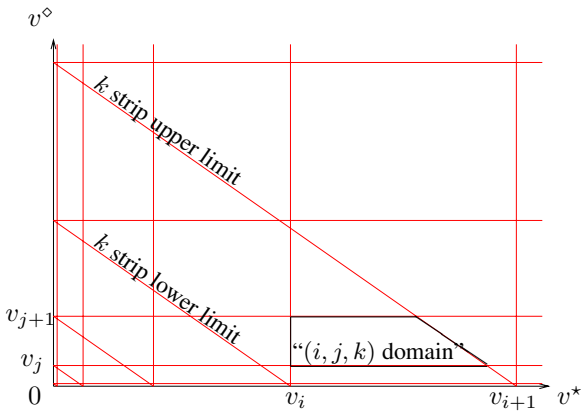

Figure 2: Coalescence terms are integrated on the "(i,j,k) domains"

where $\bar{\mathbf{F}}_k$ is the "classical" averaged drag force per unit mass on a section (Greenberg et al. 1993; Laurent and Massot 2001) :

$$\bar{\mathbf{F}}_k = \frac{\mathbf{U} - \bar{\mathbf{u}}_k}{\overline{\tau}_k}, \quad \frac{1}{\overline{\tau}_k} = \int_{S_{k-1}}^{S_k} \frac{\rho_l}{6\sqrt{\pi}} \frac{{}^1\kappa_k(S) S^{3/2}}{\tau(S)} \mathrm{d}S.$$

The total system thus counts twice as much equations as the number of sections.

First order coalescence terms In each section equation, the creation coalescence terms result from a double integration : on the whole colliding partner size space at the kinetic level (eq. 2) and on the concerned section at the Multi-Fluid level. Yet the second dependency will not coincide with the section after mapping the natural variables of the two precursor colliding partners. Thus splitting the integration domain thanks to the section continuity yields elementary integrals Q_{ijk}, triply indexed with the two precursor section numbers (i,j) and the destination section number (k). These domains are illustrated in Fig. 2.

In the particular case of the first order method, considering [H2] and assuming $\mathfrak{E}_{\text{coll}} = \mathfrak{E}_{\text{coal}} = 1$ (Laurent and Massot 2001), the coalescence integrals Q_{ijk} take the following form after factorizing the mass moments $m_i m_j$:

$$\begin{aligned}
{}^1\mathrm{Q}^\star_{ijk} &= \iint_{v^\star + v^\diamond \in [v_k, v_{k+1}[} {}^1\kappa_i(r^\star) {}^1\kappa_j(r^\diamond) \pi (r^\star + r^\diamond)^2 \frac{4}{3} \pi \rho_l r^{\star 3} \mathrm{d}r^\star \mathrm{d}r^\diamond \\
{}^1\mathrm{Q}^\diamond_{ijk} &= \iint_{v^\star + v^\diamond \in [v_k, v_{k+1}[} {}^1\kappa_i(r^\star) {}^1\kappa_j(r^\diamond) \pi (r^\star + r^\diamond)^2 \frac{4}{3} \pi \rho_l r^{\diamond 3} \mathrm{d}r^\star \mathrm{d}r^\diamond
\end{aligned}$$

As for the disappearance terms, they can also be computed as sums of the elementary creation integrals and must be so to ensure the conservation of matter and energy. After some algebra, the coalescence terms ${}^1\mathrm{C}_k^{m+}$, ${}^1\mathrm{C}_k^{m-}$, ${}^1\mathrm{C}_k^{mu+}$ and ${}^1\mathrm{C}_k^{mu-}$ read :

$$\begin{aligned}
{}^1\mathrm{C}_k^{m+} &= \sum_{i=1}^{I(k)} m_i \sum_{j=1}^{N} m_j \, |\bar{\mathbf{u}}_i - \bar{\mathbf{u}}_k| \, ({}^1\mathrm{Q}^\star_{ijk} + {}^1\mathrm{Q}^\diamond_{ijk}) \\
{}^1\mathrm{C}_k^{m-} &= m_k \sum_{j=1}^{N} m_j \, |\bar{\mathbf{u}}_k - \bar{\mathbf{u}}_j| \sum_{i=1}^{N} {}^1\mathrm{Q}^\star_{kji} \\
{}^1\mathrm{C}_k^{mu+} &= \sum_{i=1}^{I(k)} m_i \sum_{j=1}^{N} m_j \, |\bar{\mathbf{u}}_j - \bar{\mathbf{u}}_k| \, (\bar{\mathbf{u}}_i {}^1\mathrm{Q}^\star_{ijk} + \bar{\mathbf{u}}_j {}^1\mathrm{Q}^\diamond_{ijk}) \\
{}^1\mathbf{C}_k^{mu-} &= m_k \bar{\mathbf{u}}_k \sum_{j=1}^{N} m_j \, |\bar{\mathbf{u}}_j - \bar{\mathbf{u}}_k| \sum_{i=1}^{N} {}^1\mathrm{Q}^\star_{kji}
\end{aligned} \tag{8}$$

The integrands of the Q_{ijk} integrals depend only on size parameters r,$r^\star$ and $r^\diamond$ thanks to [H4]. This allows the Q_{ijk} integrals to be pre-calculated as soon as the section limits and the $({}^1\kappa_k)_k$ are given, i.e. once and for all at the beginning of a simulation.

1.5 Second order method

Second order size assumption The second order Multi-Fluid model is based on a two-coefficient exponential approximation of the size distribution in each section. This means that [H4] reads, for $S \in [S_{k-1}, S_k[$:

$${}^2\kappa_k(t, \mathbf{x}, S) = a_k(\mathbf{x}, t) \exp(-b_k(\mathbf{x}, t) S)$$

where $(a_k(\mathbf{x},t), b_k(\mathbf{x},t))_k$ ensures

$$\begin{cases}
\displaystyle\int_{S_{k-1}}^{S_k} {}^2\kappa_k(t, \mathbf{x}, S) \mathrm{d}S = n_k(t, \mathbf{x}) \\
\displaystyle\int_{S_{k-1}}^{S_k} {}^2\kappa_k(t, \mathbf{x}, S) \frac{\rho_l}{6\sqrt{\pi}} S^{3/2} \mathrm{d}S = m_k(t, \mathbf{x})
\end{cases}$$

The choice of an exponential function ensures the positivity of the distribution function whatever scheme is chosen. It also aims at reducing the number of sections and is well suited for evaporation, which requires mass flux information at the section boundary. On the other hand, coalescence becomes more difficult to compute if one wants to respect realizability conditions on the sections i.e. the fact that $(m_k, n_k)_k$ couples are conditioned by the section boundaries since they drive information on average droplet volume .

Equations The conservation equations for the k^{th} section now read :

$$\begin{aligned}
\partial_t n_k + \partial_{\mathbf{x}} \cdot (n_k \bar{\mathbf{u}}_k) &= {}^2\mathrm{C}_k^{n+} - {}^2\mathrm{C}_k^{n-} \\
\partial_t m_k + \partial_{\mathbf{x}} \cdot (m_k \bar{\mathbf{u}}_k) &= {}^2\mathrm{C}_k^{m+} - {}^2\mathrm{C}_k^{m-} \\
\partial_t (m_k \bar{\mathbf{u}}_k) + \partial_{\mathbf{x}} \cdot (m_k \bar{\mathbf{u}}_k \otimes \bar{\mathbf{u}}_k) &= m_k \bar{\mathbf{F}}_k + {}^2\mathbf{C}_k^{mu+} - {}^2\mathbf{C}_k^{mu-}
\end{aligned} \tag{9}$$

The total system thus counts three times as much equations as the number of sections.

Second order coalescence terms Since the time and space dependency of the size-distribution functions ${}^2\kappa_k(t,\mathbf{x},S)$ is no longer factorizable as was m_k in the first order method, the Q_{ijk} integrals must be computed at each time step in each cell on its "(i,j,k) domain". So it is numerically interesting to integrate the collision/coalescence efficiency at the same time. That is why this method is "less inappropriate" for efficiency models. Let us take the notation :

$$\Psi^{ij}(t,\mathbf{x},r^\star,r^\diamond,|\mathbf{u}^\diamond-\mathbf{u}^\star|) = {}^2\kappa_i(t,\mathbf{x},S^\star){}^2\kappa_j(t,\mathbf{x},S^\diamond)\times \pi(r^\star+r^\diamond)^2\mathfrak{E}(r^\star,r^\diamond,|\mathbf{u}^\diamond-\mathbf{u}^\star|)\ |\bar{\mathbf{u}}_i-\bar{\mathbf{u}}_j|$$

The coalescence integrals have a different homogeneity than in the first order method. They now include the number, mass or momentum information and read :

$$\begin{aligned}
{}^2\mathbf{Q}^n_{ijk} &= \iint_{v^\star+v^\diamond\in[v_k,v_{k+1}[} \Psi^{ij}(t,\mathbf{x},r^\star,r^\diamond,|\mathbf{u}^\diamond-\mathbf{u}^\star|)\mathrm{d}r^\star\mathrm{d}r^\diamond \\
{}^2\mathbf{Q}^\star_{ijk} &= \iint_{v^\star+v^\diamond\in[v_k,v_{k+1}[} \Psi^{ij}(t,\mathbf{x},r^\star,r^\diamond,|\mathbf{u}^\diamond-\mathbf{u}^\star|)\frac{4}{3}\pi\rho_l r^{\star 3}\mathrm{d}r^\star\mathrm{d}r^\diamond \\
{}^2\mathbf{Q}^\diamond_{ijk} &= \iint_{v^\star+v^\diamond\in[v_k,v_{k+1}[} \Psi^{ij}(t,\mathbf{x},r^\star,r^\diamond,|\mathbf{u}^\diamond-\mathbf{u}^\star|)\frac{4}{3}\pi\rho_l r^{\diamond 3}\mathrm{d}r^\star\mathrm{d}r^\diamond
\end{aligned}$$

The coalescence source terms ${}^2\mathbf{C}^{n+}_k$, ${}^2\mathbf{C}^{n-}_k$, ${}^2\mathbf{C}^{m+}_k$, ${}^2\mathbf{C}^{m-}_k$, ${}^2\mathbf{C}^{mu+}_k$ and ${}^2\mathbf{C}^{mu-}_k$ are still written as direct sums of the "(i,j,k) integrals" but therefore read :

$$\begin{aligned}
{}^2\mathbf{C}^{n+}_k &= \sum_{i=1}^{I(k)}\sum_{j=1}^{N} 2\,.\,{}^2\mathbf{Q}^n_{ijk}\,,\ {}^2\mathbf{C}^{n-}_k = \sum_{j=1}^{N}\sum_{i=1}^{N} {}^2\mathbf{Q}^n_{kji} \\
{}^2\mathbf{C}^{m+}_k &= \sum_{i=1}^{I(k)}\sum_{j=1}^{N}({}^2\mathbf{Q}^\star_{ijk}+{}^2\mathbf{Q}^\diamond_{ijk})\,,\ {}^2\mathbf{C}^{m-}_k = \sum_{j=1}^{N}\sum_{i=1}^{N}({}^2\mathbf{Q}^\star_{kji}+{}^2\mathbf{Q}^\diamond_{kji}) \\
{}^2\mathbf{C}^{mu+}_k &= \sum_{j=1}^{i}\sum_{k=K_L}^{K_H}(\bar{\mathbf{u}}_j{}^2\mathbf{Q}^\star_{ijk}+\bar{\mathbf{u}}_k{}^2\mathbf{Q}^\diamond_{ijk})\,,\ {}^2\mathbf{C}^{mu-}_k = \bar{\mathbf{u}}_i\,.\,{}^2\mathbf{C}^{m-}_k
\end{aligned} \tag{10}$$

1.6 Numerical strategy for coalescence

Towards computation, the main difference with the first order method is the time and space dependency of the integrals ${}^2\mathbf{Q}^n_{ijk}$, ${}^2\mathbf{Q}^\star_{ijk}$ and ${}^2\mathbf{Q}^\diamond_{ijk}$. The second order method requires indeed a costly numerical integration for each time step and space cell. We have chosen to perform these integrations with a 2D 5 point Newton-Cotes quadrature which requires $\Psi^{ij}(t,\mathbf{x},r^\star,r^\diamond,|\mathbf{u}^\diamond-\mathbf{u}^\star|)$ to be computed $5^2\times N^2_{sec}\times N_{cell}$ times per time step. The accuracy of this method on such exponential functions has been tested but will not be discussed any further.

Yet performing this integration with an advanced collision or coalescence efficiency model is now natural and hardly more costly. That's why these efficiencies have only been included in the second order method. Laurent et al. (2004) introduces a general form for coalescence efficiency formulas to be suitable for a pre-calculated first order method but no collision efficiency models can be easily implemented since they require local gas parameters. That is why the first order method here excludes such collision efficiency models.

2 Dynamic Study : the Nozzle Test Case

As a main criterion, we want to compare the two Multi-Fluid methods on their ability to describe the dynamics of a coalescing cloud. We therefore need a well-suited test case, inducing coalescence as well as size-conditioned dynamics and difficult enough to highlight the limitations of the methods.

For that purpose, we have chosen the configuration which was used in Laurent and Massot (2001) to validate the first order method compared to a reference Lagrangian solver : a 2D axisymmetrical conical decelerating nozzle, designed in such a way that it admits, for one-way coupling spray dynamics a self-similar solution. We though inject a lognormal distribution instead of a bi-modal one.

2.1 Definition of configuration

The chosen configuration is stationary 2D axisymmetrical in space and 1D in droplet size. It is described in detail in Laurent et al. (2004). Hence, only its essential characteristics are given here.

For the problem to be one-dimensional in space, conditions for straight trajectories are used and are compatible with the assumption of an incompressible gas flow. This leads to the following expression for the gaseous axial velocity U_z and the reduced radial velocity U_r/r, for $z \geq z_0$:

$$U_z = U(z) = \frac{z_0^2 U(z_0)}{z^2}, \quad \frac{U_r}{r} = \frac{U_z}{z} = \frac{z_0^2 U(z_0)}{z^3}$$

where $z_0 > 0$ is the coordinate of the nozzle entrance and the axial velocity $U(z_0)$ at the entrance is fixed. The trajectories of the droplets are also assumed straight since their injection velocity is co-linear to the one of the gas. This assumption is only valid when no coalescence occurs. However, even in the case of coalescence, it is valid in the neighborhood of the centerline.

Because of the deceleration of the gas flow in the conical nozzle, droplets are slowing down too, however at a rate depending on their size and inertia. This will induce coalescence. The deceleration at the entrance of the nozzle is taken as $a(z_0) = -2U(z_0)/z_0$; it is chosen large enough so that the velocity difference developed by the various sizes of droplets is important. Laurent and Massot (2001) chose rather large values, as well as strong deceleration, leading to extreme cases: $U(z_0) = 5$ m.s^{-1},

$z_0 = 5$ cm : these values generate a very strong coupling between coalescence and droplet dynamics. These severe conditions make the test cases under consideration very efficient tools for the numerical evaluation of the two Eulerian models. Finally please note that no efficiency law is used in this section so that the second order method remains comparable to the first order method, which lacks this sort of model. We thus assume $\mathfrak{E}_{\text{coll}} = \mathfrak{E}_{\text{coal}} = 1$ in this section.

2.2 Droplet initial distribution

The lognormal distribution is useful to characterize alumina particles in solid propergol rocket boosters. We therefore choose a lognormal distribution on the surface variable, without loss of generality. The droplets are constituted of liquid alumina, their initial velocity is the one of the gas, their initial temperature, fixed at the equilibrium temperature 3600 K (corresponding to an infinite conductivity model), does not change along the trajectories.

For the sake of the first order method accuracy, we do not want to transfer too much mass in the last section. The initial injected mass concentration is therefore taken as $m_0 = 1.0609$ kg.m^{-3}. For the same reason, the lognormal parameters are set to $S_{LN} = 1600\mu m^2$ and $\delta_{LN} = 1.5$ which corresponds to a sharp distribution centered on a radius of $11.3\mu m$. We shall yet keep in mind that the second order method can accurately treat cases where the final section hosts a significant portion of the mass whereas the first order method would need to increase the number of sections. The nozzle test case has thus been designed to meet optimal first order specifications i.e. where as much sections as possible get filled but the final section remains almost empty.

We now choose the tested numbers of sections : a 5 section test case illustrates what happens with a coarse discretization. A 13 section and a 25 section test cases prove the convergence of the method. They are compared to a 53 first order run which we use as a reference solution. The first order indeed has been fully validated compared to a lagrangian test case in Laurent and Massot (2001).

2.3 Distribution spread up results

The processing of polydispersion gives a first indication on the method's accuracy. We therefore compare the mass concentration distributions at the nozzle output to the 53 section reference test case in Fig. 3. With 5 sections, the first order strongly overestimates the size growth while the second order underestimates it. With 13 sections, the trend is the same but the error is smaller. Finally for 25 sections, we consider both methods are roughly converged. The growth overestimation of the first order method for poor size discretization brings about major consequences for the spray dynamics.

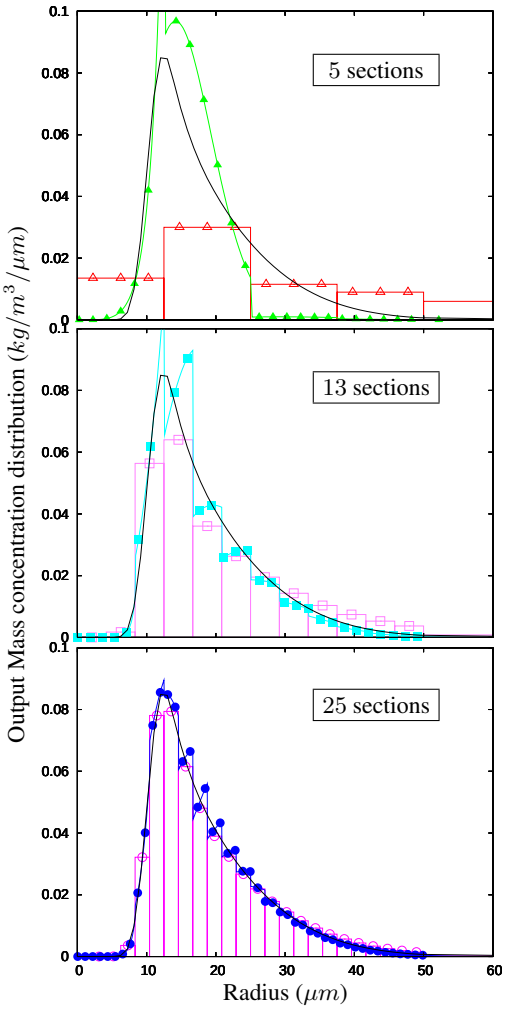

Figure 3: Mass concentration distribution at the nozzle's end computed with the first and second order methods (empty and filled symbols) and reference (black)

2.4 Spray dynamics results

Let us now appreciate the consequences of polydispersion treatment on dynamics. Fig. 4 shows the evolution of mass and number concentrations along the centerline of the nozzle computed with both Eulerian methods (5,13,25 sections) compared to the reference solutions (53 section first order method and lagrangian reference test case). For the first order case, number concentrations are computed considering section average droplet volumes given by integration of the $({}^1\kappa_k)_k$ functions : data are therefore redundant with mass concentration data. We emphasize the fact that the convergence of the

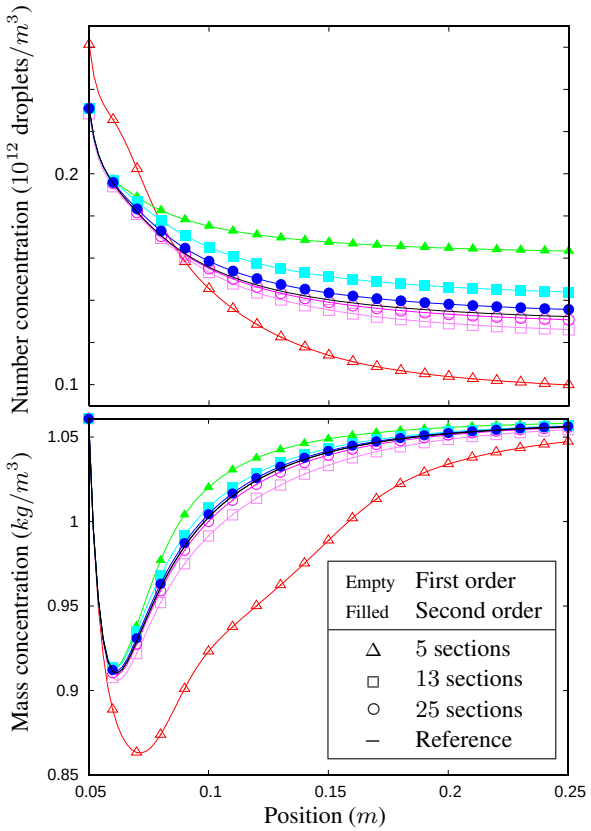

Figure 4: Number and mass concentration along nozzle for 5, 13, 25 sections and reference solution (black)

Groups (μm)	5 sections	13 sections	25 sections
G_1=[0, 12.5]	1	1 to 3	1 to 6
G_2=[12.5, 25]	2	4 to 6	7 to 12
G_3=[25, 37.5]	3	7 to 9	13 to 18
G_4=[37.5, 50]	4	10 to 12	19 to 24
G_5 ($> 50\mu m$)	5	13	25

Table 1: Composition of the five section groupings

two methods is achieved for 25 section simulations as we can see in Fig. 5, which is a zoom of Fig. 4.

To compare precisely the effect of polydispersion on dynamics, let us now consider five size intervals : they correspond to the sections in the 5 section case and are composed of section groupings in the other cases as illustrated in table 1. The evolution of the mass concentration of these groupings along the nozzle is given in Fig. 6. It is there obvious that the 5 section first order error on coalescence is severe, especially in the fifth and last grouping G_5 where no mass should be found consequently to the problem parametrization. Finally, the second order method reveals to have acceptable error with as few as 5 sections.

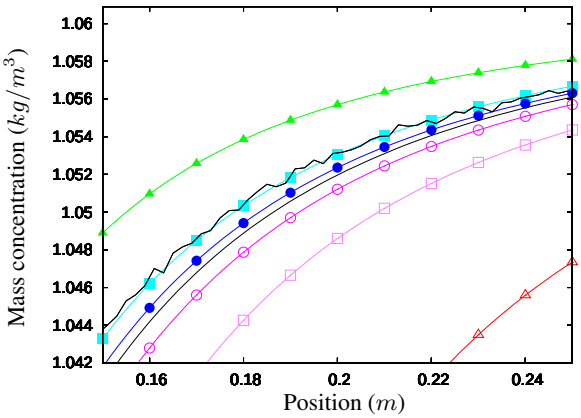

Figure 5: Zoom on the convergence of mass concentration at the nozzle's end (black : rough lagrangian validation)

	1st order MF	2nd order MF
5 sections	1 s	10 s
13 sections	1.5 s	50 s
25 sections	2 s	180 s
53 sections	5 s	n.a.

Table 2: Computational time for $10,000$ iterations on a 2.66GHz Intel Core 2 Duo CPU

2.5 Computational time

To conclude this study, table 2 recaps the duration of the different runs. It is obvious that the first order method is much faster since it is highly optimized thanks to the pre-calculation. Even when considering the 5 section second order run -which is fairly as accurate as the 13 section first order- it is 6 time slower.

Yet two restrictions must be added about the use of the first order with a thinner size space discretization. First, it is not possible to meet such a high computation speed with specific collision/coalescence laws. Second for typical solid propulsion simulations, each section requires the resolution of an unsteady 3D pressureless Euler-type system so that solving for coalescence is no longer the limiting step. Thus increasing the number of section becomes a costly operation, restraining the profit of the first order method.

3 Coalescence Experimentation : the D'Herbigny Test Case

In this section, we provide further validation for the second order Multi-Fluid method, by comparing it to a 1D experiment on collision/coalescence efficiency models. Moreover this configuration provides tough testing for Eulerian models because it deals with bimodal size dis-

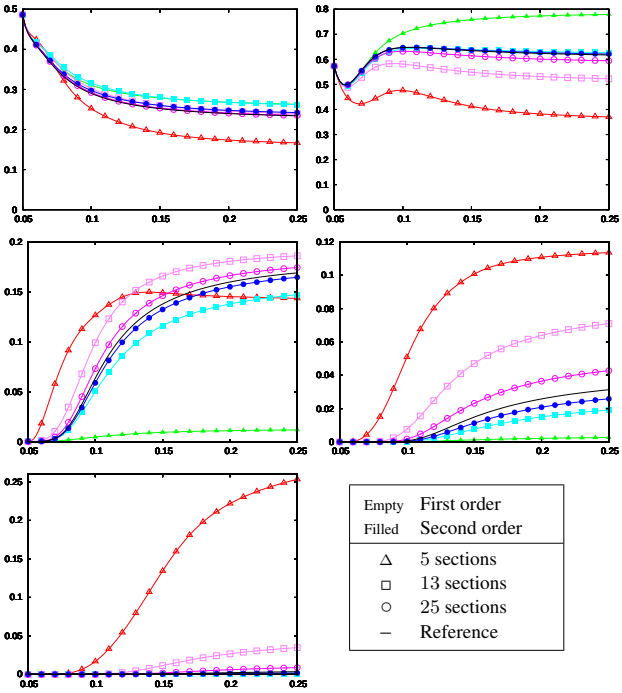

Figure 6: Evolution of mass concentration in the four finite section groupings and in the last section for 5, 13 and 25 sections

tributions. Indeed, modal distributions (i.e. monodisperse or discrete distributions) are rather suited for the Lagrangian point of view while they introduce stiff size distributions in Eulerian modelling.

3.1 The D'Herbigny collision efficiency experiment

In the D'Herbigny experiment, coalescence is studied through the growth of a bigger droplet falling through a fog of smaller droplets. Details about the experimental device and conditions can be found in D'Herbigny and Villedieu (2001) and in Fig. 7.

In this experiment, the average injection radius of the bigger droplets is $r_2 = 150\mu m$ thanks to piezoelectric injector which is fairly accurate. The smaller droplets, composing the fog, have a radius $r_1 \in [2\mu m, 4\mu m]$. The two types of droplets have an approximately constant velocity difference of $3m/s$ along the tunnel. One can therefore compute the values of the k parameter used in the Langmuir-Blodgett and Beard-Grover collision efficiency models. They are given in table 3.

Moreover, the collisional Reynolds number Re is around 60 which is comparable to the values in the Ariane 5 P230 booster. This range of values (moderate Re and low k) is supposed to be favorable to the Beard-Grover law.

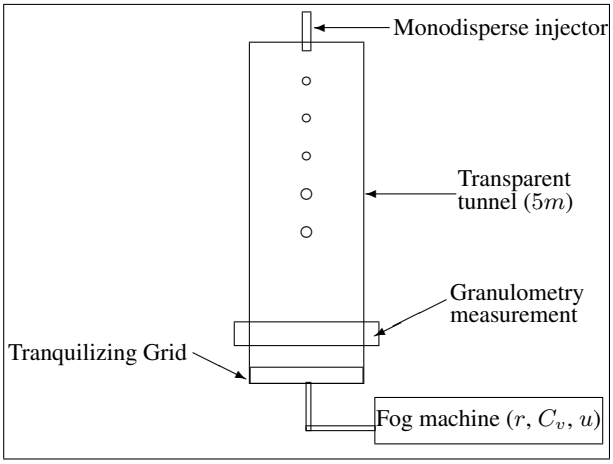

Figure 7: D'Herbigny experimental device

r_1	$2\mu m$	$2,5\mu m$	$3\mu m$	$3,5\mu m$	$4\mu m$
k	0.78	1.22	1.75	2.39	3.12

Table 3: Collision parameter k values in the D'Herbigny experiment

3.2 Results

Droplet radius growth study D'Herbigny and Villedieu (2001) provide an analytic formula to estimate the Sauter mean radius growth Δr_2 of the bigger droplets when assuming a small growth and a constant velocity difference :

$$\Delta r_2 = \alpha \overline{\mathfrak{E}_{\text{coll}}} C_v \tag{11}$$

where C_v is the volume fraction of the fog, $\overline{\mathfrak{E}_{\text{coll}}}$ the average collision efficiency and α results from the integration of the impact parameter. As a first step, we thus perform the simulation with a constant velocity of $3m/s$ to fit the analytical result. Experimental, analytical and simulation results are given in Fig. 8.

The first conclusion is that collision efficiency laws have a strong impact on radius growth, here undermining it up to 50%.

The second conclusion is a positive validation of both laws implemented in the second order Multi-Fluid Method. According to D'Herbigny and Villedieu (2001), this constant velocity study also concludes that Langmuir-Blodgett law is most suited for rocket chamber-like conditions.

Method numerical stability The third conclusion of these simulations is that the method allows robust and accurate simulation of stiff distributions. Indeed the simulations are converged for a rough number of 100 iterations and provide a self-similar solution which means low diffusion in the size phase space.

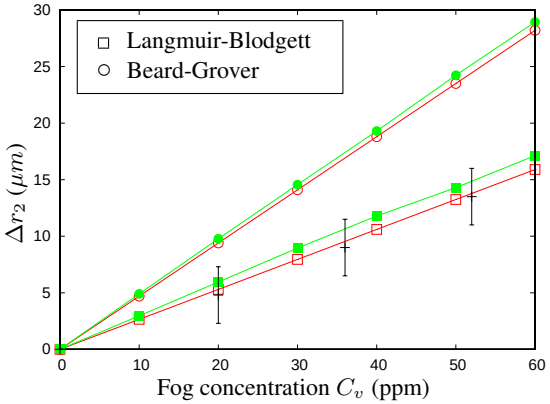

Figure 8: Radius growth Δr_2 after $5m$ through a C_v concentration fog (empty red : Analytical; filled green : Second order simulation with constant velocity; black : Experimental).

3.3 Discussion on velocity

As a second step, let us revise the constant velocity assumption. On the one hand, droplets do reach a terminal velocity, i.e. the drag force compounds the weight but this limit velocity increases with the droplet size since the drag force increases like the droplet surface while the weight increases like the droplet volume. On the other hand, collisions with a static fog induce a momentum dilution i.e. a significant slow down. We can see the evolution of the effective velocity as calculated by the code when gravity, drag force and coalescence momentum transfer are enabled in Fig. 9. The droplet velocity tends to be slightly smaller than the terminal velocity because of momentum dilution.

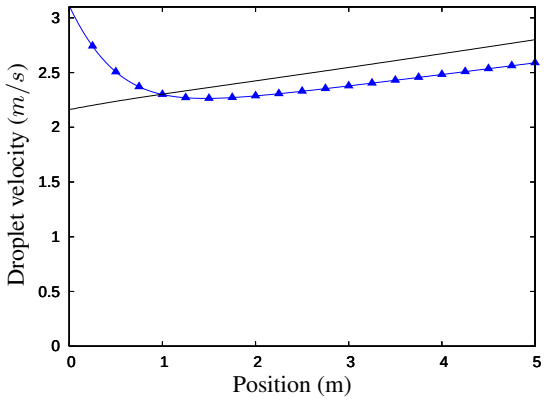

Figure 9: Velocity along the tunnel with gravity, drag force and coalescence momentum transfer (blue triangles) and terminal velocity for the corresponding Sauter Mean Radius (black)

Yet the consequences of velocity on coalescence are not obvious. First let us neglect efficiency laws. The coalescence rate per unit time linearly increases with the velocity difference (eq. 2) but linearly decreases with the time spent in the tunnel so that it vanishes in the final growth formula (eq. 11). In fact radius growth for a fixed length travel only depends on the number of collisions i.e. fog concentration and travel length, assuming a fairly constant cross section. However when considering efficiency laws, the velocity difference plays a role since it controls the way smaller droplets can dodge the bigger ones. For instance eq. 11 depends linearly on an averaged collision efficiency factor strongly conditioned by velocity difference as shown in Fig. 1.

The new simulation results with full dynamics is given in Fig. 10. It shows that the Beard Grover efficiency correlation is not so bad while the average velocity might have been slightly overestimated in D'Herbigny and Villedieu (2001). As a final restriction, please note that no coalescence efficiency law has been used ($\mathfrak{E}_{\text{coal}} = 1$) which suggests not to conclude on which collision efficiency law to use.

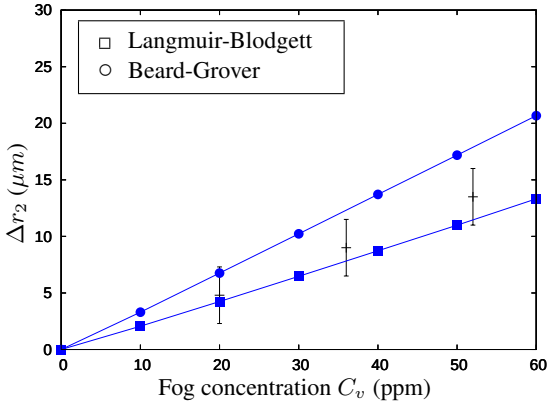

Figure 10: Radius growth Δr_2 with velocity resolution (filled blue : Second order simulation; black : Experimental)

3.4 Conclusion on the model and methods

The previous results confirm that Eulerian Multi-Fluid methods can be used to simulate accurately the size-distribution evolution of a coalescing spray and its size-conditioned dynamics. The first order method provides, with a reasonable number of sections (between 10 and 20), extremely fast results since it is highly optimized. The second order Multi-Fluid method provides good results with a very coarse size-space discretization (as few as 5 sections). If both methods can include coalescence efficiency models, only the second order method easily provides collision efficiency models. The corresponding laws can significantly reduce the particle growth rate which is experimentally observed so that these efficiency models are essential to capture the physics of coalescence.

4 Rocket booster simulation

In this section, we conclude the study by achieving a 2D complex simulation of a rocket booster chamber and nozzle which experiences the meeting of a parietal injection of gas and small alumina droplets resulting from the combustion of propergol and an axial two-phase flow carrying bigger droplets supposedly coming from priorly injected, burnt and coalesced particles. The upper part of the chamber generating these bigger droplets is not solved.

4.1 The CEDRE code

The CEDRE code has been developed at ONERA for several years to provide a multiphysics comprehensive tool for energetics problems in aeronautics. The main feature is the combination of a non structured spatial solver with models as varied as multiphase flows, multispecies chemistry, thermal conduction, radiation, wall-film models, etc. The coupling can be one or two-way. As for the disperse phase, CEDRE includes a Lagrangian and two Eulerian methods i.e. a multi-class and the second order Multi-Fluid method studied here. Only the Lagrangian and the Multi-Fluid methods provide coalescence models.

4.2 Configuration

The 2D rocket booster simulation is performed on a simplified configuration, yet featuring the main difficulties of solid propulsion typical flows i.e. parietal injection and a supersonic nozzle. It takes place on a deformed-structured 1500 cell mesh (Fig. 11, top). When seeking a two-phase stationary flow solution, one usually takes a converged gas flow field as an initial state. With a total rate of flow of 10 $kg.s^{-1}.m^{-2}$ from the wall (propellant combustion) and the head end (upstream flow), this gas flow involves extemely high velocity gradients in the nozzle (Fig. 11, middle), which will induce size-conditioned droplet dynamics as studied in section two. The simulation strictly speaking starts when injecting the disperse phase : a monomodal $5\mu m$ radius wall injection represents the droplets resulting from recently burnt aluminum particles, directly expelled from the propellant grain, and another roughly monomodal distribution around $20\mu m$ is injected on the axis to model the previously coalesced droplets (Fabignon et al. 2003). For the purpose of our simulation, the injected volume fractions (more or less 5.10^{-5}) approximate correctly typical rocket booster conditions and preserve the dilute spray hypothesis.

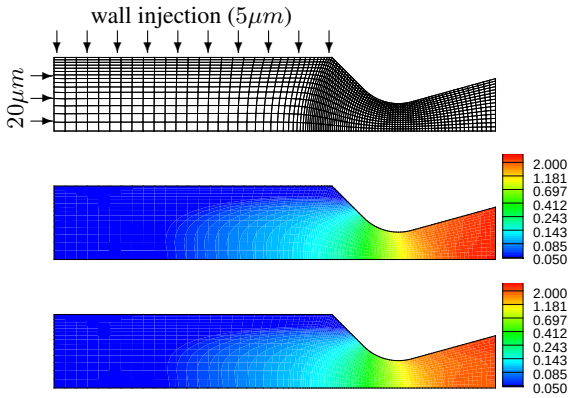

Figure 11: Top : Deformed-structured 1500 cell mesh (Arrows : injection zones); Middle : Gaseous Mach number without particle; Bottom : with particles

4.3 Results

For the disperse phase, we choose a 5 section discretization (0, 12.5, 25, 37.5 and 50 μm) as in section two. A 10^{-2} s time interval is required to allow the first droplets to reach the end of the nozzle. With a 10^{-6} s time step ($10,000$ iterations), we perform a 1 h single processor AIX platform computation. The stationary volume fractions for the five sections are displayed in Fig. 12.

First, the disperse phase has an impact on the gas flow since we perform a two-way coupling simulation. Specific impulse loss can indeed be observed with the nozzle Mach number decrease in Fig. 11, bottom. Second, we do note bigger particle creation in Fig. 12 : coalescence occurs as soon as the two injected types of droplets meet since the third section gets filled with significant volume fractions ($\approx 10^{-5}$) in the chamber. Third, bigger droplets are created in the nozzle eventhough acceleration there induces a strong volume fraction dilution. In pursuance of section two, section 5 is left almost empty with a volume fraction around 10^{-10} (the colormap is different from the other section ones); yet a different discretization could be used to activate this section thus increasing size accuracy.

4.4 Remaining Numerical difficulties in solid propulsion

The final simulation of this paper illustrates the ability of Multi-Fluid models to provide in a reasonable time fairly accurate information on polydisperse coalescing sprays in complex geometry gas flows. The above results however suggest several possible improvements, among which reducing computational time and considering more physical phenomena.

Typical advanced rocket booster simulations are unsteady and performed on more complex meshes : they can include from $10,000$ cells to millions of cells for

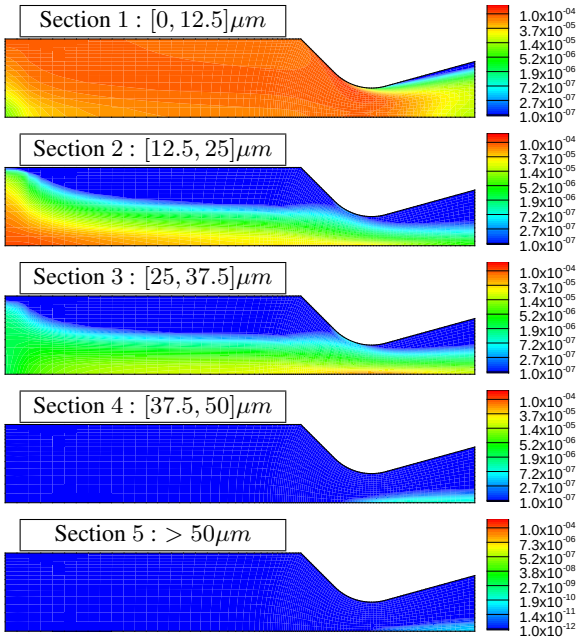

Figure 12: Dispersed phase volume fractions

3D meshes. Highly optimized code and multiprocessor computations (with several spatial domains for instance) are therefore required. In our constant time step simulation, the CFL condition is driven by the flow in the nozzle but the gap between the chamber and the nozzle stay times makes most of the early time steps too short and therefore uselessly numerous. An adaptative time step method considering both phases including operator splitting could prevent from ill-suited time steps.

Physically, high velocity gradients in the nozzle induce droplet secondary break-up which strongly undermines droplet growth. Since it is out of the scope of this paper, this phenomenon has been neglected but its modelling reaches two requirements : specific impulse computation is subject to the precise knowledge of droplet size after the nozzle throat and experimental data on alumina size distribution mainly consist of ejected material which has encountered complete break-up process. Developpement of fragmentation models for the Eulerian Multi-Fluid method has been achieved in Dufour (2005).

Finally, the main drawback of such methods comes from the monokinetic hypothesis : it forbids droplet crossings which should occur on the centerline of our simulation and induces instead a droplet accumulation artifact due to the momentum averaging on the symmetry axis. On more advanced solid propulsion unsteady configurations, dedicated to hydrodynamic instability studies for instance, high-inertia droplets ejected from vortices need a multivelocity treatment which advanced high order moment methods can provide as developed in Kah et al. (2010).

5 Conclusions

In this paper, we provide a comprehensive validation of a Eulerian, second order in size, method for solving two-phase polydisperse coalescing flows. The conclusion of this study is that the existing method is able to simulate accurately the dynamics of such flows with less sections than the first order method as demonstrated in section two yet in a slower way. It is however the only Eulerian Multi-Fluid method including validated advanced collision efficiency models, which are crucial for rocket booster studies. Finally, the method is practically efficient in rocket booster simulation contexts; moreover reducing the number of required sections can be profitable to the computational time of such simulations. The remaining limitations underlined in the final section require though further developments but the method can bear such improvements.

6 Acknowledgments

The present research was done thanks to a Ph. D. Grant from DGA, Ministry of Defence (M. S. Amiet, Technical Monitor). The authors also thank G. Dufour and T. Fontfreyde for their preliminary contribution to the second order method in the CEDRE code.

References

B. Abramzon and W.A. Sirignano. Droplet vaporization model for spray combustion calculations. *Int. J. Heat Mass Transfer*, 32:1605–1618, 1989.

P. Achim. *Simulation de collisions, coalescence et rupture de gouttes par une approche lagrangienne: application aux moteurs à propergol solide*. PhD thesis, Université de Rouen, 1999.

A. A. Amsden, P. J. O'Rourke, and T. D. Butler. Kiva ii, a computer program for chemically reactive flows with sprays. Technical Report LA-11560-MS, Los Alamos National Laboratory, 1989.

K. V. Beard and S. N. Grover. Numerical collision efficiencies for small raindrops colliding with micron size particles. *J. of atmospheric sciences*, 31:543–550, 1974.

G. A. Bird. Molecular gas dynamics and the direct simulation of gas flows. *Oxford Science Publications*, 42, 1994.

F. Bouchut. On zero pressure gas dynamics. In *Advances in kinetic theory and computing*, pages 171–190. World Sci. Publishing, River Edge, NJ, 1994.

P.R. Brazier-Smith, S.G. Jennings, and J. Latham. The interaction falling water drops : coalescence. *Proceedings of the Royal Society*, 326:393–408, 1972.

S. De Chaisemartin. *Modèles eulériens et simulation numérique de la dispersion turbulente de brouillards qui s'évaporent*. PhD thesis, Ecole Centrale de Paris, 03 2009. http://tel.archives-ouvertes.fr/tel-00443982/en/.

F. X. D'Herbigny and P. Villedieu. Etude expérimentale et numérique pour la validation d'un modèle de coalescence. Technical Report RF1/05166 DMAE, ONERA, 2001.

G. Dufour. *Modélisation multi-fluide eulérienne pour les écoulements diphasiques à inclusions dispersées*. PhD thesis, Université Paul Sabatier Toulouse III, 2005.

J. K. Dukowicz. A particle-fluid numerical model for liquid sprays. *J. Comput. Phys.*, 35(2):229–253, 1980.

J. Dupays, Y. Fabignon, P. Villedieu, G. Lavergne, and J. L. Estivalezes. Some aspects of two-phase flows in solid-propellant rocket motors. In *Solid Propellant Chemistry, Combustion, and Motor Interior Ballistics*, volume 185 of *Progress in Astronautics and Aeronautics*. AIAA, 2000.

Y. Fabignon, O. Orlandi, J.F. Trubert, D. Lambert, and J. Dupays. Combustion of aluminum particles in solid rocket motors. *AIAA Paper 2003-4807*, July 20-23 2003. In 39th AIAA/ASME/SAE/ASEE Joint Propulsion Conference and Exhibit , Huntsville, Tx.

J. B. Greenberg, I. Silverman, and Y. Tambour. On the origin of spray sectional conservation equations. *Combustion and Flame*, 93, 1993.

J. J. Hylkema. *Modélisation cinétique et simulation numérique d'un brouillard dense de gouttelettes. Application aux propulseurs à poudre*. PhD thesis, Ecole Nat. Supérieure de l'Aéronautique et de l'Espace, 1999.

J. J. Hylkema and P. Villedieu. A random particle method to simulate coalescence phenomena in dense liquid sprays. In *Lecture Notes in Physics*, volume 515, pages 488–493, Arcachon, France, 1998. Proc. 16th Int. Conf. on Num. Meth. in Fluid Dyn.

D Kah, F Laurent, L Fréret, S De Chaisemartin, R Fox, J Reveillon, and M Massot. Eulerian quadrature-based moment models for dilute polydisperse evaporating sprays. *Flow Turbulence and Combustion*, pages 1–26, 04 2010. http://hal.archives-ouvertes.fr/hal-00449866/en/.

P. Kuentzmann. *Aérothermochimie des suspensions*. Gautier-Villars Editeur, 1973.

I. Langmuir. The production of rain by a chain reaction in cumulous clouds at temperatures above freezing. *J. Meteor.*, 5:17–192, 1948.

F. Laurent. Numerical analysis of Eulerian multi-fluid models in the context of kinetic formulations for dilute evaporating sprays. *M2AN Math. Model. Numer. Anal.*, 40(3):431–468, 2006.

F. Laurent and M. Massot. Multi-fluid modeling of laminar poly-dispersed spray flames: origin, assumptions and comparison of the sectional and sampling methods. *Comb. Theory and Modelling*, 5:537–572, 2001.

F. Laurent, M. Massot, and P. Villedieu. Eulerian multi-fluid modeling for the numerical simulation of coalescence in polydisperse dense liquid sprays. *J. Comp. Phys.*, 194:505–543, 2004.

M. Massot. *Eulerian Multi-fluid models for polydisperse evaporating sprays*, chapter III of "Multi-Phase Reacting Flows: Modelling and Simulation", pages 79–123. CISM Courses and Lectures No. 492. Springer, 2007. Editors D.L. Marchisio and R. O. Fox,.

M. Massot, F. Laurent, D. Kah, and S. De Chaisemartin. A robust moment method for evaluation of the disappearance rate of evaporating sprays. *to appear in SIAM J. of App. Math.*, 2010. http://hal.archives-ouvertes.fr/hal-00332423/en/.

P. O'Rourke. *Collective drop effects on vaporizing liquid sprays*. PhD thesis, Los Alamos National Laboratory 87545, University of Princeton, 1981.

M. Rüger, S. Hohmann, M. Sommerfeld, and G. Kohnen. Euler/Lagrange calculations of turbulent sprays: the effect of droplet collisions and coalescence. *Atomization and Sprays*, 10(1):47–81, 2000.

B. Tòth. *Two-phase flow investigation in a cold-gas solid rocket motor model through the study of the slag accumulation process*. PhD thesis, Université Libre de Bruxelles, 2008.

I. M. Vasenin, R. K. Narimanov, A. A. Glazunov, N. E. Kuvshinov, and V. A. Ivanov. Two-phase flows in the nozzles of solid rocket motors. *J. Propulsion and Power*, 11(4):583–592, 1995.

F. A. Williams. Spray combustion and atomization. *Phys. Fluids*, 1:541–545, 1958.

F. A. Williams. *Combustion Theory (Combustion Science and Engineering Series)*. ed F A Williams (Reading, MA: Addison-Wesley), 1985.

Y. B. Zel′dovich. Gravitational instability : an approximate theory for large density perturbations. *Astronomy and Astrophysics*, 5:84–89, 1970.